IEEE Access
Multidisciplinary ⋮ Rapid Review ⋮ Open Access Journal

Received August 26, 2021, accepted September 5, 2021, date of publication September 9, 2021,
date of current version September 20, 2021.

Digital Object Identifier 10.1109/ACCESS.2021.3111319

Development of Numerical Modeling and Temperature Controller Optimization for Internal Heating Vacuum Furnace

YUEFEI WANG[1,2] AND ZHEN LIU[2], (Member, IEEE)
[1]School of Mechanical and Marine Engineering, Beibu Gulf University, Qinzhou 535011, China
[2]Department of Integrated Systems Engineering, Nagasaki Institute of Applied Science, Nagasaki 851-0193, Japan

Corresponding author: Zhen Liu (zliu999@hotmail.com)

This work was supported in part by the 2021 Guangxi University's Young and Middle-Aged Teachers' Basic Research Ability Improvement Project under Grant 2021KY0442, and in part by Guangxi Ship Digital Design and Advanced Manufacturing Engineering Technology Research Center, Beibu Gulf University.

ABSTRACT Compared with traditional fire refining to remove impurities, the vacuum distillation method has the advantages of simple steps, high direct yield and no pollution to environment. The vacuum furnace, as the main equipment of vacuum distillation method, is widely used in resource regeneration and new material fabrication. To solve the engineering problems that the temperature control system of internal heating vacuum furnace has large time delay and real time temperature is hard to be measured precisely, the paper proposes an approach to model and calculate the temperature values for each node in the furnace at no-load. A disturbance model for the temperature field of the system by the vacuum furnace itself is developed. This methodology is useful for modeling the temperature field and the temperature control when implementing the experiment such as the vacuum reduction of MgO or the vacuum evaporation of Pb-Sn alloy using this furnace. To verify the effectiveness of the proposed method, experimental equipment is set up and experiments are done on the heating process of the internal heating vacuum furnace. Compared with the simulation results, the experimental results verify the correctness of the numerical modeling approach. In addition, a hybrid controller with Smith's predictive proportion integral differential (PID) based on particle swarm optimization (PSO) algorithm is developed. The simulation results show that the controller has the advantages of no overshoot, short rise time and adjustment time compared with the conventional controller. It solves the pure delay for this temperature control model effectively.

INDEX TERMS Hybrid controller, internal heating vacuum furnace, temperature control model.

I. INTRODUCTION

The internal heating vacuum furnace is one of the main equipment of the vacuum distillation method, which has wide use in the regeneration of secondary resources, extraction of precious metals from binary alloys, and development of new materials [1], [2]. In industrial production, the temperature in the furnace is difficult to measure when it is in operating mode, and the temperature control model has the characteristics of model uncertainty and serious time-delay [3], [4]. Hence, it is hard to reach the control accuracy by traditional control methods. PID control algorithm is widely used in industry. The optimal PID parameter self-tuning controller has the advantages of good robustness, high reliability, and simple algorithm [5]. However, due to the limitations of the PID controller structure, the control effect of conventional PID controllers cannot be satisfied with large time-delay systems [6].

Most researchers often use the Smith predictor method to solve the time-delay system, but Smith predicts controller's parameters are too sensitive, and therefore its anti-jamming ability and robustness [7]. It is found that the problem of nonlinearity, strong inertia, time-varying, and pure delay for electric vacuum furnace could be effectively solved by PID genetic algorithm [8]. Particle Swarm Optimization (PSO) is a global optimization algorithm based on group intelligence and works well for the optimization of continuous systems [9]. Shi and Eberhart [10] introduce the concept of

The associate editor coordinating the review of this manuscript and approving it for publication was Lei Wang.

inertia weight to the original version of PSO, in order to balance the local and global search during the optimization process. Mausri Bhuyan *et al.* [11] have compared the system robustness for PID controllers tuned with sine-cosine algorithm (SCA) and PSO algorithms in a power coordination application to hybrid microgrids and found that the former outperformed the latter. Ratnaweera and Halgamuge [12] introduces a novel parameter automation strategy for PSO and two further extensions to improve its performance after a predefined number of generations. Nevertheless, the traditional particle swarm optimization algorithm is easy to fall into the local optimum and cannot achieve the optimization goal in time, it cannot ensure the PID model to achieve the best performance. Guimin Chen [13] proposes to use the concave function for learning factors improvement. The purpose of this method is to speed up the change of c_1c_1 and c_2 at early time so that the algorithm can get to the local search faster, and the experimental results prove that the method is feasible. However, these methods lack diversity and tend to converge on local extremes too early, and the optimization effect is not obvious. Therefore, the development of a hybrid controller based on the PSO algorithm to tune the PID controller parameters is important for the dead-time system [14]. The main contributions for this paper are as follows:

(1) Use the internal heating vacuum furnace (see Figure 1) to implement the experiment which measures the temperature of representative positions inside the furnace.

(2) Model the temperature process with the measured temperature data.

(3) Design PSO-based hybrid controllers and explore variable learning factors of PSO for local models to improve the overall performance.

The paper is organized as follows. In Section 2, the physical model and experimental modeling for the internal heating vacuum furnace are introduced, and a hybrid controller based on the PSO algorithm is designed. In Section 3, temperature measurement experiments are established to verify the correctness for the numerical modeling approach. The effect of the hybrid controller with different learning factors is explored using MATLAB (MathWorks, Natick, Massachusetts, USA, Nagasaki Institute of Applied Science purchased the license). Finally, the conclusion is given in Section 4.

II. NUMERICAL MODELING AND HYBRID CONTROLLER

A. STRUCTURE AND WORKING PRINCIPLE OF INTERNAL HEATING VACUUM FURNACE

The furnace is mainly composed of Q235 steel shell, evaporation pan, graphite condenser, graphite heating column, and water-cooling system (see Figure 1).

The graphite electric column in the furnace core is used for heating element. In the reaction process, the phase transformation of metal is carried out from top to bottom by the evaporation pan. That is, the metal turns into metal vapor at the evaporation dish, which turns from gas to liquid as it flows to the condensation lid. Finally, it flows along the condensation lid to the liquid collector [15]. The flowing steam not only increases the evaporation surface but also enhances the thermal efficiency by increasing the churning of the fluid and decreases the phase transition temperature. The entire smelting process is short, does not require the addition of chemical reagents, does not pollute the environment, has a high metal recovery rate, and has low capital investment and processing costs. Compared with the electrolytic separation of alloys, this furnace has obvious economic and social benefits.

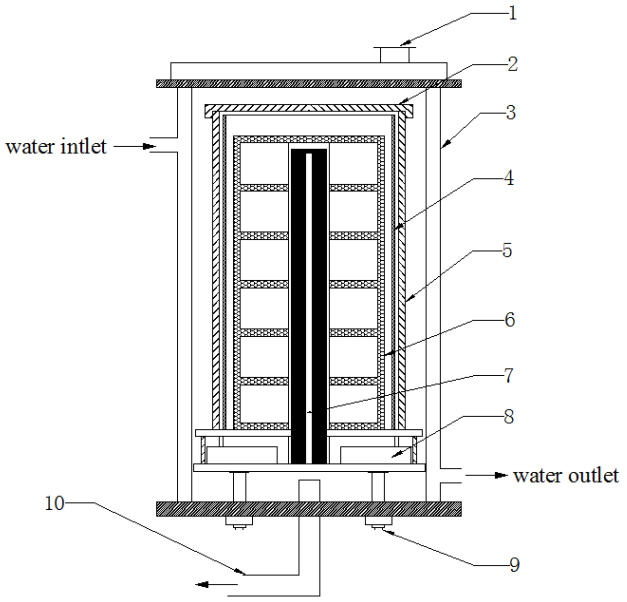

FIGURE 1. The schematic diagram of the induction heating system (1-observation hole; 2-graphite cover; 3-cold water furnace cover; 4-condensation cap; 5-thermal shroud; 6-crucible; 7-Electric pillar; 8-open-top container; 9-water-cooled electrode bar; 10-vacuum pump).

The water-cooling system plays an extremely important role in the whole smelting process. It not only keeps the furnace body at a relatively low temperature but also makes the furnace temperature difference between the top and bottom so that the metal molecules evaporated can be enriched on the container to achieve the binary metal separation.

B. MODELING PROCESS

As it is difficult to measure the internal temperature during reaction stage with a working vacuum furnace, we tried to solve the problem by numerical modeling approach. We simulated and analyzed the vacuum furnace model using ANSYS (software copyrighted by Guangxi Ship Digital Design and Advanced Manufacturing Engineering Technology Research Center) [16]. Due to the main view of the vacuum furnace is axisymmetric, the right half of the front view is modeled for simulation. The dimension diagram for the vacuum furnace (see Figure 2). The main material properties and parameters related to each part of the vacuum furnace are given (see Table 1). T1, T2 and T3 are the positions where the thermocouple sensors will be installed in the subsequent

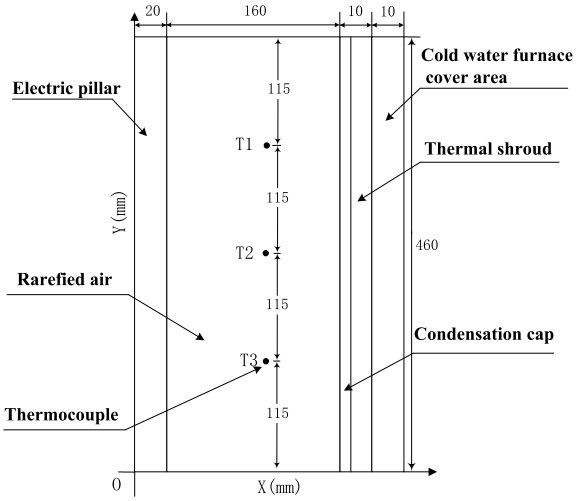

FIGURE 2. Dimension drawing of vacuum furnace and thermocouple (Right half front view, mm).

TABLE 1. Material parameters of the vacuum furnace.

Material	Graphite	Q235 steel
Density ($Kg \cdot m^{-3}$)	500	7850
Thermal conductivity ($W \cdot m^{-1} \cdot K^{-1}$)	129	(See Table 3)
Emissivity	0.97	0.75
Specific heat capacity ($J \cdot g^{-1} \cdot K^{-1}$)	710	480

experiments. They are also the isothermal surfaces to be calculated in the numerical modeling.

For the purpose of describing the temperature field distribution inside the furnace during the whole heating process and simulating the general work conditions, some assumptions are fixed.

- As preliminary research, this paper only experiments on the internal heating multi-stage continuous vacuum furnace under no-load condition, so the graphite crucibles are removed during the experiment.
- Assuming that the height of the graphite electric column in the vacuum furnace is equal to the height of the condensation hood, and the angular coefficient of radiative heat transfer between the graphite column and the furnace wall is considered equal everywhere.
- The interior of the vacuum furnace is in a micro vacuum state, so only the thermal radiation between the electric pillar, thermal shroud and the water-cooling furnace cover are considered.
- The rarefied air in the reaction zone is evenly distributed.
- Set the simulation environment pressure to $80Pa$.

The thermal conductivity of Q235 steel differs at different temperatures, so when setting the material parameters of furnace shell, the partial value of the Q235 steel thermal conductivity (see Table 3) within the heating up stages in vacuum furnace [17].

The simulation steps are as follows: First, in ANSYS, the parameters (see Table 1) and (see Table 3) are set for the vacuum furnace model (see Figure 2). Then, divide the mesh, define the cell division size as 0.005. Third, apply the temperature load and solve. The initial environment temperature is set at 25°C, the water-cooling system temperature at 70°C, and the maximum temperature of the heating element at 1500°C, respectively. Applied emissivity load: 0.97 for graphite electric column and 0.75 for Q235 steel, respectively. Applied temperature load: heating element for T0 = 1500°, the water-cooled wall for T1 = 70°C, respectively. Define the Stephen Boltzmann constant as 5.669e-8, the temperature offset TOFFST = 273, define the convergence tolerance of 0.01 in the radiation solution option, select the iterative solution algorithm, and define the angle coefficient solution option (select plane analysis), respectively [18]. Set the number of iterations to 1000. Because the default maximum number of iterations in ANSYS is 25, and the calculation will end when there is no convergence after 25 iterations, so it is necessary to increase the iterations number. Then save the disk and solve the problem. Finally, there is the post-processing for the results. The obtained results are processed to obtain the simulated temperature field distribution when the steady-state is reached, and the temperature distribution for the simulation calculation results is (see Figure 3). The temperature is mapped along the furnace $x = 200mm$ direction path, picking up the axial three equal nodes (see Figure 3a). Extract and display the temperature values of three nodes on this path, nodes T1, T2, T3 simulation calculation results (see Figure 3b). The temperature distribution cloud chart for thermal radiation shows that the temperature distribution in furnace decreases radially from the electric pillar to the furnace cover, and the temperature decreases from top to bottom. The simulation results of nodes T1, T2 and T3 in the insulation stage are 873.234°C, 826.477°C and 792.306°C respectively (see Figure 3b).

In order to validate the numerical modeling, we executed thermometry experiments for the vacuum furnace. Installation dimensions of the thermocouple sensors (see Figure 2), and 3-D layout (see Figure 4).

15 high-temperature thermocouples of dual platinum-rhodium are installed in the vacuum furnace, with a total of three layers. Each layer is composed of one thermocouple close to the graphite column and four thermocouples on the concentric circle (see Figure 4). Besides, a feedback thermocouple is assembled at the bottom to provide feedback signal. After the thermocouple is fixed, the wounds are sealed with high-temperature rubber sealing hedge, which ensures the sealing of the wound under the negative pressure. The experimental vacuum furnace is connected to three-phase AC power supply by the thyristor. Temperature controller system is to control the heating electric power by controlling the thyristor's energizing time, thus changing the heating electric power and controlling the temperature rise. The controller input is the temperature deviation value, the output is the on-time for the thyristor. Set the upper limit of power output

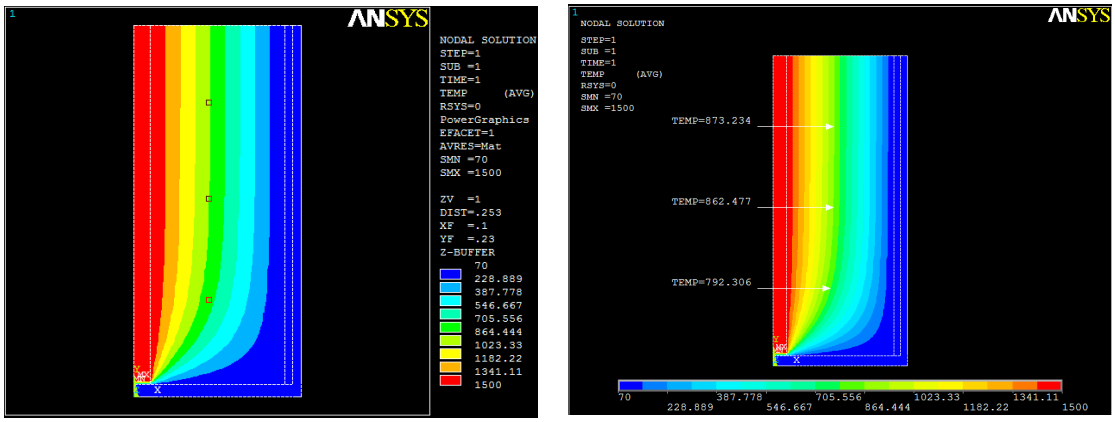

(a) Distribution of test nodes

(b) Simulation results for node temperature

FIGURE 3. Thermal radiation simulation diagram of vacuum furnace model (Right half front view, °C).

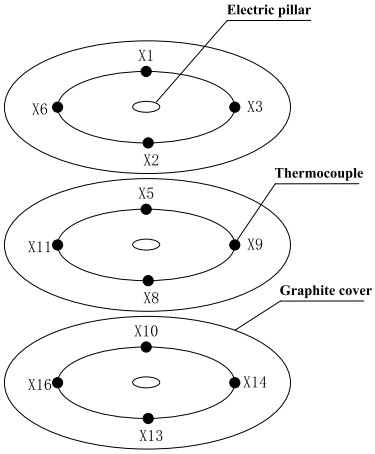

FIGURE 4. Schematic diagram of thermocouple position in furnace.

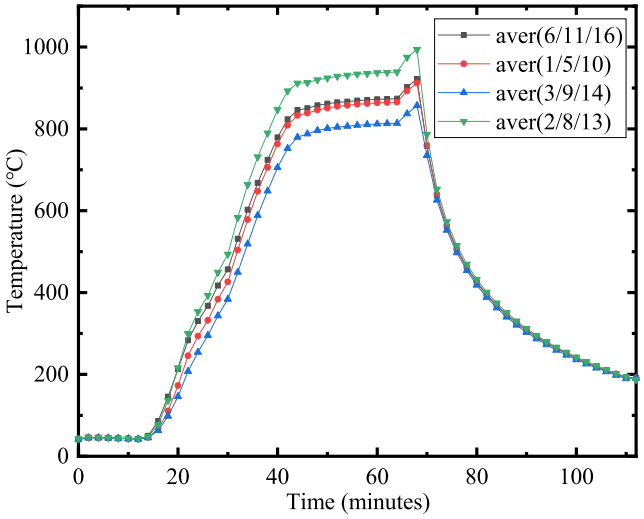

FIGURE 5. The average temperature curve of thermocouple group (X2, X8, X13), group (X3, X9, X14), group (X1, X5, X10), and group (X6, X11, X16) measured in the vacuum furnace within 0-112 minutes.

is 50%. The Siemens S7-300 controller is used for real-time temperature acquisition, and the temperature data measured by 15 high-temperature thermocouples are obtained from 0 to 112 minutes, recorded every two minutes.

To obtain the real-time changes for the temperature field in furnace and reduce the measurement error, so take the average values of thermocouples in the furnace vertical direction (see Figure 5). The average temperature value curve of the four thermocouples show that the measured temperature values are relatively stable over 48-66 minutes. Considering that the four thermocouple groups are installed at the same isothermal surface, and the temperature curves trend are consistent in general. The vacuum furnace enters the heat preservation stage at about 48 minutes. The thermocouples are in the relatively stable period of the heat preservation stage at 50-58 minutes. Therefore, take the average curve of the four groups with temperature values from 0 to 65 minutes as the heating process.

The isothermal surface measured temperature curve (see Figure 5) shows that: during 48-66 minutes, the temperature for the reaction area in the furnace chamber is relatively stable, taking into account the four groups of thermocouples installed in the same isothermal surface, and the temperature curve is approximately the same direction, so it can be considered that the vacuum furnace in about 48 minutes into the insulation stage. Within 50-58 minutes, it is in a relatively stable holding period. The temperature data for three sets of thermocouples are (see Table 2).

C. PSO-BASED HYBRID CONTROLLER

The paper uses the step response method to identify the temperature control system of the internal heat multi-stage continuous vacuum furnace. The temperature curves (see Figure 5) measured by the four group thermocouples is approximately the same direction, and the simulation has been proved to be correct by the experiment. Therefore, take the mean temperature values measured by the

TABLE 2. Partial temperature data measured by thermocouples.

Group Number	Thermocouples	50min (°C)	52min (°C)	54min (°C)	56min (°C)	58min (°C)	Average Value (°C)	Isothermal Surface Temperature (°C)
1	X2	931.4	935	937.4	940.5	942.3	816.2	869.7
	X3	878	881	883.4	886	887.7	883.2	
	X1	874.4	878.1	880.4	882.9	884.5	880.1	
	X6	893.4	896.9	899.3	902.2	903.8	899.1	
2	X8	953.3	959.9	962.1	965	966.5	961.4	857.9
	X9	753.6	756.7	758.9	761.1	762.7	758.6	
	X5	768	771.8	774.5	777.1	779	774.1	
	X11	934.3	936.4	937.6	939.4	940.3	937.6	
3	X13	887.6	890.9	893.1	895.8	897.4	892.9	812.2
	X14	771.7	775	777.1	779.4	780.8	776.8	
	X10	811.3	814.4	816.6	818.7	820.2	816.2	
	X16	757.1	760.7	763.2	765.7	767.4	762.8	

four group thermocouples. In addition, the heating, rise and heat preservation values are taken and normalized (see Figure 6).

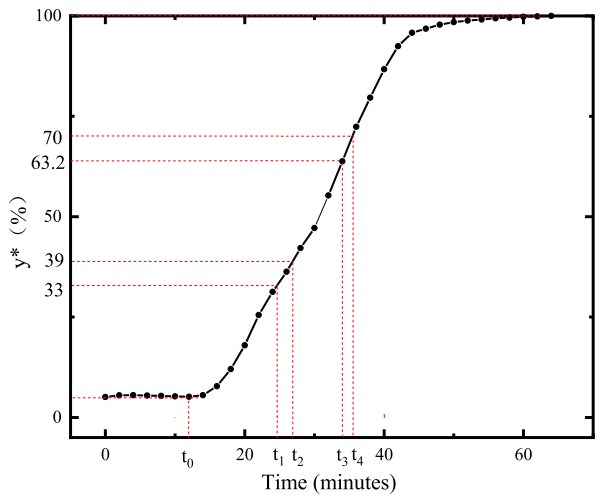

FIGURE 6. Normalized temperature rise curve in vacuum furnace.

The slope of the unit step response for the vacuum furnace temperature object (see Figure 6) is approximately 0 when $t = 0$, and the slope gradually increases as it increases. When it is greater than 32 minutes, the slope gradually decreases. Therefore, the system can be described by using first-order inertia plant with time delay model

$$K_0 = \frac{y(\infty) - y(0)}{\Delta u} = \frac{900 - 50}{0.5} = 1700, \tag{1}$$

where K_0 is the static amplification factor. When the input signal is unit step signal, the solution of $y^*(t)$ is

$$y^*(t) = \begin{cases} 1 - e^{-\frac{t-\tau}{T_0}} & (t \geq \tau) \\ 0 & (t < \tau) \end{cases}. \tag{2}$$

Then, t_1 and t_2 corresponding to different time $y^*(t_1)$ and $y^*(t_2)$ are selected for simultaneous solution (see Figure 6), T_0 and τ are determined as

$$\left.\begin{aligned} y^*(t_1) &= 1 - e^{-\frac{t_1-\tau}{T_0}} \\ y^*(t_2) &= 1 - e^{-\frac{t_2-\tau}{T_0}} \end{aligned}\right\}, \tag{3}$$

When $t_2 > t_1 > \tau$, taking the natural logarithm of both sides for Equation (3), we get

$$\left.\begin{aligned} T_0 &= \frac{t_2 - t_1}{ln[1 - y^*(t_1)] - ln[1 - y^*(t_2)]} \\ \tau &= \frac{t_2[1 - y^*(t_1)] - t_1 ln[1 - y^*(t_2)]}{[1 - y^*(t_1)] - ln[1 - y^*(t_2)]} \end{aligned}\right\}, \tag{4}$$

After calculation and verification, the transfer function is identified as

$$G(s) = \frac{K_0 e^{-\tau s}}{T_0 s + 1} = \frac{850 e^{-156s}}{936s + 1}. \tag{5}$$

Equation (5) represents the temperature control model during no-load operation of the internal heating vacuum furnace. The control process is a non-linear, with large inertia and large time-delay [19].

The main drawback for traditional PID tuning is that the overshoot is relatively large, the response speed is also slower, the self-adaptive ability is poor, and the control effect is still not ideal. In dynamic process, due to these characteristics, the output lags behind input, and it is impossible to completely follow the input change. Aiming to solve these problems, we developed a hybrid controller with Smith's predictive PID based on PSO algorithm (see Figure 7). The hybrid controller requires pre-tuning PID individual parameters under Smith's predictive control structure. The blue area (see Figure 8) presents setting the optimization-seeking bounds for the PID parameters in PSO algorithm to reduce the computation time and improve the optimization quality.

PSO is a random search algorithm based on group collaboration developed by simulating birds foraging for food.

TABLE 3. Thermal conductivity of Q235 steel at different temperatures.

Temperature (℃)	100	300	500	700	800	860	900	1000
Thermal conductivity $(W \cdot m^{-1} \cdot K^{-1})$	46.41	40.23	31.208	19.433	28.049	27.961	29.522	31.238

TABLE 4. Measured and simulated values of three isothermal surfaces.

Isothermal Surface	T1(X1/X2/X3/X6)	T2(X5/X8/X9/X11)	T3(X10/X13/X14/X16)
Simulation value (℃)	873.234	826.471	792.306
Measured value (℃)	869.66	857.9	812.21
Correction value (℃)	-0.8223	0.2878	0.7146
Deviation (℃)	-4.3963	31.7168	20.6186
Absolute percentage error (%)	0.506	3.696	2.536

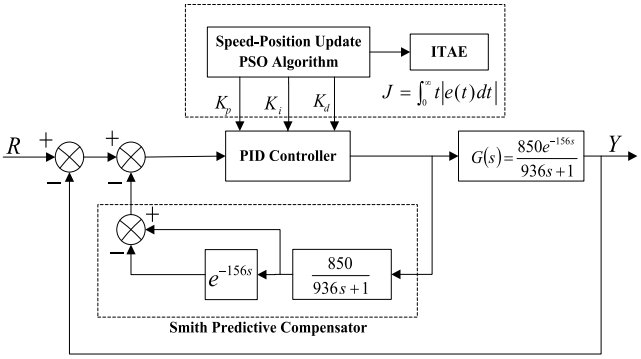

FIGURE 7. Schematic diagram for the hybrid controller based on Smith predictor and PSO algorithm.

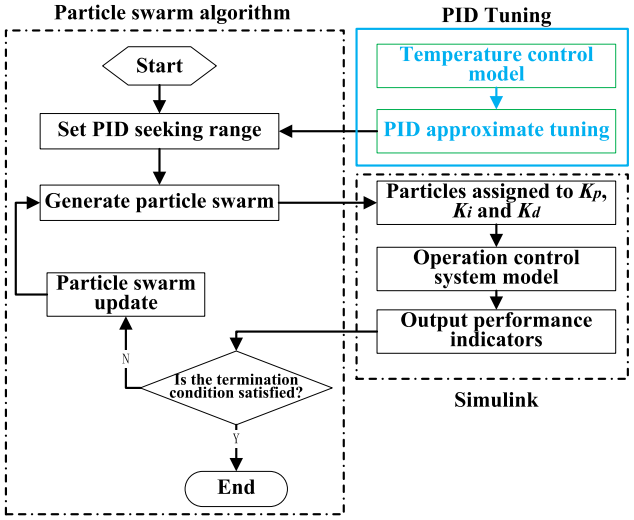

FIGURE 8. Flowchart for the hybrid controller based on PSO algorithm.

The algorithm uses the velocity-position model, and the particle swarm velocity-position update formula is as follows

$$v_{id} = w * v_{id} + c_1 r_1 (p_{id} - x_{id}) + c_2 r_2 \left(p_{gd} - x_{id}\right), \quad (6)$$

$$x_{id} = x_{id} + v_{id}, \quad (7)$$

where r_1 and r_2 are two separately generated uniformly distributed random numbers in the range [0,1], c_1 and c_2 are learning factors[20]. The algorithm repeats the velocity and position of the new particles according to Equation (7) and (8) until the maximum number of cycles is reached, or a predetermined minimum fitness threshold is satisfied, at which point the result is the optimal solution. According to Equation (6), the particle velocity update is mainly determined by three components.

The first part of Equation (6) is the inertia, which reflects the motion habit of the particle and represents the tendency of the particle to maintain its previous velocity. The second part is cognitive, which reflects the memory of the particle's historical experience and represents the tendency of the particle to approach the best position in its history [21]. The third part is social cognition, which responds to the group-historical experience of collaborative cooperation and knowledge sharing among particles and represents the tendency of particles to approach the best position in the group or threshold history. Therefore, the learning factors c_1 and c_2 in PSO reflect the information exchange between particle populations [22].

Although the PSO algorithm converges quickly and has low computational complexity, it is prone to diversity loss and falls into local optimum [23]. With the traditional PSO algorithm, the learning factor is set to $c_1 = c_2 = 2$. For the purpose of enriching particle diversity and improving the case of overripening and falling into local extremes, we tried to design the equal random learning factor improvement approach to obtain better convergence [24]. Therefore, the relatively better search results are selected as the random interval for the learning factor. The novel PSO is implemented in Equation (6), the values of c_1 and c_2 are randomly taken from 0.5 to 2.0, respectively. The equations are as follows

$$c_1' = c_2' = 1.3 + (2.0 - 1.3)\, rand\,(), \quad (8)$$

Take Equation (8) into Equation (6) and get

$$v_{id} = w * v_{id} + c_1' r_1 (p_{id} - x_{id}) + c_2' r_2 \left(p_{gd} - x_{id}\right). \quad (9)$$

TABLE 5. PID controller parameters under different algorithms.

Algorithm	PSO-Smith-PID	PSO-Smith-PID	PSO-Smith-PID	PID-Smith	PID
Learning Factors	c_1=c_2=2	c_1=c_2=1.7	c_1=c_2=0.5	/	/
V-Fitness	1.609×10^7	5.407×10^6	6.208×10^6	/	/
K_p	1.350×10^{-3}	1.500×10^{-2}	1.410×10^{-2}	1.856×10^{-3}	1.856×10^{-3}
K_i	9.907×10^{-6}	1.600×10^{-5}	1.500×10^{-5}	3.000×10^{-6}	3.000×10^{-6}
K_d	0.0095	0.0018	0.0046	0.06698	0.06698

where Equation (9) and Equation (7) together form the equal random learning factor PSO algorithm in this paper. We performed this novel PSO based on the designed PSO-Smith-PID (PSO & Smith predictive control & PID control) hybrid controller to explore whether it contributes to the optimization of PID parameters. To obtain optimal control results, the novel algorithm optimizes the PID parameters when the ITAE standard is reached (see Figure 8).

The paper performs simulation experiments on the temperature control model for the internal heating vacuum furnace. Firstly, the PID parameters are pre-tuned to reduce the PSO algorithm's optimizing range for the PID parameters. Then, the PSO learning factors (e.g. 0.5, 1.7 and 2.0) generated by Equation (9) are optimized to determine the optimal parameter values for K_p, K_i and K_d of the PID controller in real-time until it reaches the ITAE standard (see Table 5). Finally, the optimized PID parameters are assigned to the hybrid controller in Simulink.

III. RESULTS AND DISCUSSION

To validate the numerical modeling approach, the temperature values measured from the experimental results in Part II B (see Table 2) are extracted for the period 48-66 minutes, where the temperature in the reaction zone is stable. The equipment for the experiment mainly includes the internal heating vacuum furnace system and the control system (see Figure 9).

To reduce the error, the curve is selected in the relatively smooth 50-58 min period, and the 12 data groups corresponding to the three nodes are averaged. The relative error is calculated using Equation (10). The measured and simulated values for the three isothermal surfaces (see Table 6).

$$\sigma_e = \frac{T_m + T_C - T_S}{T_m + T_c} \tag{10}$$

where σ_e denotes relative error, T_m denotes measured value, T_C denotes correction value, T_S denotes simulation value.

The maximum relative error between the simulated temperature values and the experimentally measured values at the three isothermal surfaces (see Table 6) is 3.696%, the minimum relative error is 0.506%, and the average relative error is 1.909%. Among them, at the isothermal surfaces T2 and T3, the error between the simulated calculated values and the measured values is larger than at T1. The reason for the larger values here is that the four thermocouples installed on the isothermal surfaces of T2 and T3 may be inserted too shallowly in the actual measurement and deviate from the coordinate position, causing the measured temperature value to be lower compared with the expected value. However, considering that the error of the average temperature is within the acceptable range, and each group temperature curve of thermocouples is nearly the same. Therefore, the data measured in the experiment are reliable.

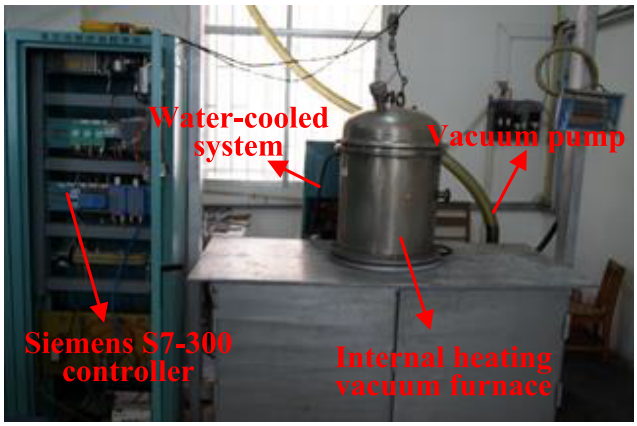

FIGURE 9. Internal heating vacuum furnace system and control system for experiment.

TABLE 6. Measured and simulated values of three isothermal surfaces.

Isothermal surface	T1(X1/X2/X3/X6)	T2(X5/X8/X9/X11)	T3(X10/X13/X14/X16)
Simulation value(℃)	873.234	826.471	792.306
Measured value(℃)	869.66	857.9	812.21
Correction value(℃)	-0.8223	0.2878	0.7146
Deviation (℃)	-4.3963	31.7168	20.6186
Absolute percentage error (%)	0.506	3.696	2.536

Then, we simulated the hybrid controller for different learning factors of the PSO algorithm and obtained the step response curves (see Figure 10). For the temperature control model under no-load, using MATLAB to experiment with the PSO-Smith-PID hybrid controller and the optimal learning factor is $c_1 = c_2 = 0.5$, and the PID parameter values (see Table 5).

The step response curves for the several controllers (see Table 7) shows that the rise time of PSO-Smith-PID ($c_1 = c_2 = 0.5$) controller is 834.3s shorter than Smith-PID controller. Except for the PID controller, which produces

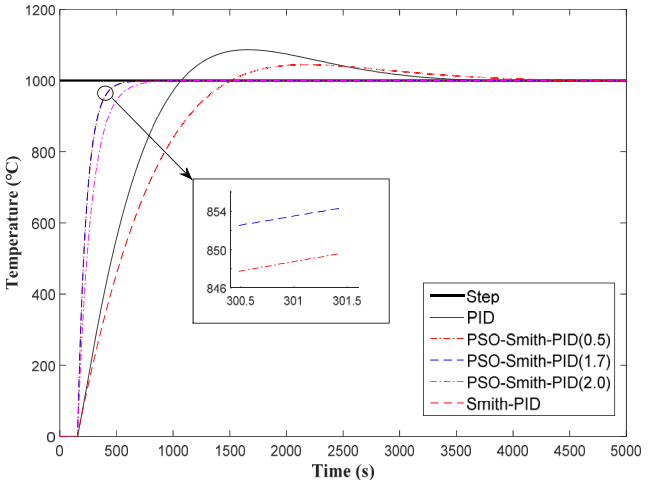

FIGURE 10. Step response of five controllers in the vacuum furnace model.

TABLE 7. The dynamic performance indexes for different temperature control systems.

	PID	Smith-PID	PSO-Smith-PID(2.0)	PSO-Smith-PID(1.7)	PSO-Smith-PID(0.5)
Rise time (s)	1071	1509	902.7	682.3	674.7
Steady-state error (°C)	1.4	0	0	0	0
Overshoot (σ%)	8.7	4.4	0	0	0
*Adjustment time (s)	3746	4716	952.9	870.4	704.5

∗ Allowance error is ±1°C.

a steady-state error of 1.4°C, none of the controllers produces steady-state errors. The overshoot is 8.7% for the PID controller, 4.4% for the Smith-PID controller, and no overshoot for the three PSO-Smith-PID controllers. The shortest adjustment time for PSO-Smith-PID ($c_1 = c_2 = 0.5$) is 704s, and the longest adjustment time for Smith-PID controller is 4716s.

Hence, Smith predictor-based PID controller reduces the overshoot compared to conventional PID controller, but the former requires a longer adjustment time. Note that the PSO-optimized hybrid controller both eliminates overshoot and significantly reduces the rise time. This indicates that the PSO algorithm has a significant improvement on the time-lagged system and effectively improves the dynamic control of the system. Although this paper adopts pre-tuned PID parameters to reduce the optimization time and shrinks the search range, PSO optimization still consumes a longer time compared to the conventional controller.

Overall, the PSO algorithm could effectively improve the control quality for Smith predictive PID controller. However, it was found that improving the learning factor of PSO, although it can further optimize the PID parameters, has little meaningful impact on practical engineering. In addition, the temperature inside the furnace is difficult to detect accurately in real time owing to the requirement of ensuring a vacuum at approximately 80Pa when the vacuum furnace is in work. The temperature field of the experimental vacuum furnace was simulated using ANSYS and the temperature values were obtained for all space locations inside the furnace. Then, in order to measure the temperature inside the furnace accurately, we drilled holes in the experimental furnace at the calibrated position and inserted 15 platinum rhodium high temperature thermocouples to measure the temperature values at the calibrated position inside the furnace. The comparison shows that the simulation results are basically consistent with the experimental test results, with a relative error between 2.5% and 3.7%.

IV. CONCLUSION

In the working process of vacuum furnace, because of the different types of smelting alloys, the operating conditions are not constant and the model parameters may fluctuate. By obtaining the perturbation of the temperature field by the vacuum furnace itself, the accuracy of the temperature field obtained when the furnace is performing different operations is improved. These problems were solved using numerical modeling approach. Then, the feasibility for the numerical modeling approach was validated by experiments: the maximum relative error between the simulated temperature values and the experimentally measured values at the three isothermal surfaces was 3.696%; the minimum relative error was 0.506%, and the average relative error was 1.909%, with errors within the engineering allowable range. In addition, a hybrid PSO-Smith-PID controller was developed to optimize the control quality after the identification for temperature control system of internal heating vacuum furnace, and the simulation experiment results showed that PSO-Smith-PID hybrid controller shortened the rise time up to 834.3°C, the steady-state error and overshoot were negligible, and the adjustment time was shortened up to 4011.5 seconds. The control quality was significantly improved. Our work may provide new temperature detection methods for the smelting of different alloys. Using numerical modeling approach to research the temperature field distribution when smelting different alloys with the vacuum furnace, as there are many engineering challenges to be solved, is also our next major work. The heat transfer mode for vacuum furnaces is different from the normal furnace. It is of practical significance to study how to improve the uniformity for the temperature distribution and how to measure the distribution of the temperature field in the furnace.

REFERENCES

[1] X. Hao, J. Gu, N. Chen, W. Zhang, and X. Zuo, "3-D numerical analysis on heating process of loads within vacuum heat treatment furnace," *Appl. Thermal Eng.*, vol. 28, nos. 14–15, pp. 1925–1931, Oct. 2008.

[2] L. Zimmermann, P. H. Blard, P. Burnard, S. Medynski, R. Pik, and N. Puchol, "A new single vacuum furnace design for cosmogenic ^{3}He dating," *Geostandards Geoanalytical Res.*, vol. 36, no. 2, pp. 121–129, Jun. 2012.

[3] M. Moshtaghi and S. M. Abbasi, "Effect of vacuum degree in VIM furnace on mechanical properties of Ni-Fe-Cr based alloy," *Trans. Nonferrous Met. Soc. China*, vol. 22, no. 9, pp. 2124–2130, 2012.

[4] B.-J. Sun and B. Xiao, "Mechanical properties of diamond grinding discs brazed in a continuous-belt tunnel furnace or vacuum furnace," *Int. J. Adv. Manuf. Technol.*, vol. 89, nos. 5–8, pp. 1379–1386, Mar. 2017.
[5] S. M. H. Mousakazemi and N. Ayoobian, "Robust tuned PID controller with PSO based on two-point kinetic model and adaptive disturbance rejection for a PWR-type reactor," *Prog. Nucl. Energy*, vol. 111, pp. 183–194, Mar. 2019.
[6] W. Xu, J. Zhang, and R. Zhang, "Application of multi-model switching predictive functional control on the temperature system of an electric heating furnace," *ISA Trans.*, vol. 68, pp. 287–292, May 2017.
[7] Q. Z. Liu and S. Y. Wang, "Research on improved internal model control method for large time-delay process," *Control Eng. China*, pp. 1–6, 2020, doi: 10.14107/j.cnki.kzgc.20200122.
[8] D. Lu, J. X. Wang, and J. F. Li, "The temperature control of electric furnace based on PID genetic algorithm," *Adv. Mater. Res.*, vols. 490–495, pp. 828–834, Mar. 2012.
[9] F. Marini and B. Walczak, "Particle swarm optimization (PSO). A tutorial," *Chemometrics Intell. Lab. Syst.*, vol. 149, pp. 153–165, Dec. 2015.
[10] Y. Shi and R. Eberhart, "A modified particle swarm optimizer," in *Proc. IEEE Int. Conf. Evol. Comput., IEEE World Congr. Comput. Intell.*, May 1998, vol. 49, no. 5, pp. 69–73.
[11] M. Bhuyan, D. C. Das, and A. K. Barik, "A comparative analysis of DSM based autonomous hybrid microgrid using PSO and SCA," in *Proc. IEEE Region Symp. (TENSYMP)*, Jun. 2019, pp. 765–770.
[12] A. Ratnaweera, S. K. Halgamuge, and H. C. Watson, "Self-organizing hierarchical particle swarm optimizer with time-varying acceleration coefficients," *IEEE Trans. Evol. Comput.*, vol. 8, no. 3, pp. 240–255, Jun. 2004.
[13] G. M. Chen, J. Y. Jia, and Q. Han, "Study on the strategy of decreasing inertia weight in particle swarm optimization algorithm," *J. Xi'an Jiaotong Univ.*, vol. 40, no. 1, pp. 53–57, 2006.
[14] E. Y. Bejarbaneh, A. Bagheri, B. Y. Bejarbaneh, S. Buyamin, and S. N. Chegini, "A new adjusting technique for PID type fuzzy logic controller using PSOSCALF optimization algorithm," *Appl. Soft Comput.*, vol. 85, Dec. 2019, Art. no. 105822.
[15] H. Wan, B. Xu, B. Yang, J. Zhao, and Y. Dai, "The impurities distribution and purification efficiency of high-purity aluminum preparation by zone melting in vacuum," *Vacuum*, vol. 171, Jan. 2020, Art. no. 108839.
[16] Q. Zhu, W. Wu, Y. Yang, Z. Han, and Y. Bao, "Finite element analysis of heat transfer performance of vacuum glazing with low-emittance coatings by using ANSYS," *Energy Buildings*, vol. 206, Jan. 2020, Art. no. 109584.
[17] X. Li, L. Zhang, Y. Sun, B. Jiang, R. Zhang, X. Li, and N. Yang, "Investigation on steam injection condition in refining vacuum furnace," *Chem. Eng. Sci.*, vol. 135, pp. 509–516, Oct. 2015.
[18] P. C. S. Kumar, R. Naveenkumar, S. K. L. Moorthy, M. Meignanamoorthy, and M. Ravichandran, "Heat transfer analysis for different materials of ball bearing using ANSYS," *Mater. Today Proc.*, vol. 12, no. 17, 2020, doi: 10.1016/j.matpr.2020.10.944.
[19] O. W. Abdulwahhab, "Design of a complex fractional order PID controller for a first order plus time delay system," *ISA Trans.*, vol. 99, pp. 154–158, Apr. 2020.
[20] J. Zhao, T. Li, and J. Qian, "Application of particle swarm optimization algorithm on robust PID controller tuning," in *Proc. Int. Conf. Natural Comput.* Berlin, Germany: Springer, 2005, pp. 948–957.
[21] J.-S. Chiou and M.-T. Liu, "Numerical simulation for fuzzy-PID controllers and helping EP reproduction with PSO hybrid algorithm," *Simul. Model. Pract. Theory*, vol. 17, no. 10, pp. 1555–1565, Nov. 2009.
[22] Z. H. Ren and J. Wang, "Accelerate convergence particle swarm optimization algorithm," *Control Decis.*, vol. 26, no. 2, pp. 201–206, 2011.
[23] C. S. Rao, S. Santosh, and D. R. V, "Tuning optimal PID controllers for open loop unstable first order plus time delay systems by minimizing ITAE criterion," *IFAC-PapersOnLine*, vol. 53, no. 1, pp. 123–128, 2020.
[24] S. Mehta, M. Singh, and R. Pamula, "Analysis of min-max algorithm and PSO algorithm for data clustering," in *Proc. Int. Conf. Big Data Manage.*, 2020, pp. 23–27.

YUEFEI WANG received the M.S. degree from the Institute of Information Engineering and Automation, Kunming University of Science and Technology, China. He is currently pursuing the Ph.D. degree with the Department of Integrated Systems Engineering, Nagasaki Institute of Applied Science, Japan. From 2015 to 2019, he worked as a Teacher with the Department of Automation, Beibu Gulf University, China, and worked on passive control and robotics. He is currently with Applied Simulation Technology working mainly on intelligent controller.

ZHEN LIU (Member, IEEE) received the Ph.D. degree in information science from Tohoku University, Japan. He is currently a Professor with the Graduate School of Engineering, Nagasaki Institute of Applied Science, Japan. His current research interests include computational intelligence, cyber security, big data and data mining, and welfare engineering. He is a member of IEEE Computer Society, Association for Computing Machinery (ACM), The Japanese Society for Artificial Intelligence (JSAI), Information Processing Society of Japan (IPS), and The Institute of Electronics, Information and Communication Engineers (IEICE).